Dynamics of polymeric liquids using polarization-modulated laser Raman scattering

L. A. Archer and G. G. Fuller
Department of Chemical Engineering, Stanford University, Stanford, CA 94305, USA

and L. Nunnelley
IBM Corporation, General Products Division, San Jose, CA 95193, USA
(Received 18 July 1991; revised 11 September 1991; accepted 25 September 1991)

A new experimental technique, 'polarization-modulated laser Raman scattering' (PMLRS), is presented for the study of the dynamics of polymeric materials subjected to transient flows. A detailed analysis of the experiment based on Jones–Mueller matrix calculus is presented. Jones and Mueller matrices that take into account the integrated effect of the deformed sample's birefringence are developed for a Raman scattering element, using either the 0° or 180° scattering geometries. To test the predictions of the theory a Raman scattering system, based on high-speed phase modulation (50 kHz) of the incident light coupled with phase-sensitive detection, has been developed. This system is also capable of simultaneously measuring birefringence. Single-step reversal extension and step strain experiments were conducted using a polyisobutylene melt. Experiments were done using the Raman scattered light associated with the ν stretching vibration of C–H groups present in the specimen. The results obtained indicate that the Raman signal ratios all depend on the second- and fourth-order moments of the orientation distribution function of polymer segments and on the sample's birefringence.

(Keywords: dynamics; polymeric liquids; Raman spectroscopy; birefringence)

INTRODUCTION

Spectroscopic, microrheological techniques that are capable of isolating the dynamics of specific components in a polymer blend can provide invaluable information about the relationship between the microstructure and rheology of these materials. To date, methods such as infra-red dichroism, depolarized fluorescence and n.m.r. have been used for this purpose. Recently, following the initial work of Bower[1], polarized laser Raman scattering has been applied successfully to the study of molecular orientation induced in polymeric materials by stretching[2–4] and by extrusion[5]. In these studies the Raman spectra of the deformed polymer specimen are collected using various combinations of the polarization direction of the incident and scattered light relative to the stretching direction, as well as various scattering geometries. The measured spectral intensities are related to the principal eigenvalues of the Raman scattering tensor in a molecule-fixed coordinate system through the orientation distribution function of molecular segments. Using this procedure both second-order ($\langle P_2(\cos\theta)\rangle$) and fourth-order moments ($\langle P_4(\cos\theta)\rangle$) of the segment orientation distribution function have been successfully determined. However, because the modulation of the polarization states of the incident and scattered light was manual, the required measurements were rather tedious and slow, making polarized laser Raman scattering unsuitable for studying time-dependent variations in polymer segment orientation. In this paper we present the theory and preliminary experimental data for a high-speed modulation scheme that makes it possible to study time-varying molecular orientations using Raman scattering. This technique will henceforth be referred to as 'polarization-modulated laser Raman scattering' (PMLRS). Compared to other spectroscopic methods that have seen recent application in rheometry, PMLRS offers important advantages, such as high spatial resolution, greater flexibility in both the nature and sizes of the polymer specimens that can be studied and the potential ability to determine both second- *and* fourth-order moments of the segment orientation distribution function. The latter information is important in the dynamics of highly extended chains and multicomponent polymer systems for which Gaussian statistics may no longer apply.

REVIEW OF THE MEASUREMENT OF POLYMER LIQUID DYNAMICS

Although PMLRS can be used to study the dynamics of any transparent polymeric liquid, in this study we apply this method to a polyisobutylene melt of amorphous, flexible chains. The description of the dynamics of even this simple class of materials is challenging and is treated thoroughly in several recent books (Doi and Edwards[6], Larson[7] and Bird *et al.*[8]). Briefly, the goal of such theories is to predict the conformation of a chain such as the one depicted in *Figure 1*.

0032-3861/92/173574-08

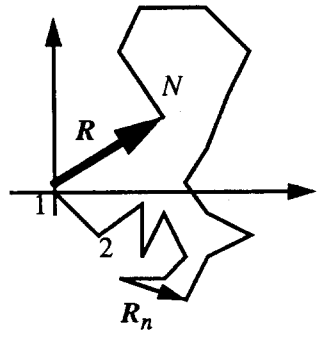

Figure 1 Bead–rod model of a flexible chain

Here the chain is represented as a sequence of beads connected by rods (or springs) that are located in space by the set of vectors $\{\boldsymbol{R}_n\}$, where the index n runs from 1 to N, N being the number of statistical subunits per chain. The conformation of the chain is then described through a probability distribution function, $\psi(\{\boldsymbol{R}_n\})\,d\boldsymbol{R}_1 \ldots d\boldsymbol{R}_n \ldots d\boldsymbol{R}_N$, which prescribes the probability that the chain will have a given conformation. Once this function is determined, bulk properties such as the stress and refractive index tensors can be calculated. A primary motivation of the present development is to provide measures of the moments of this distribution function that can be used to advance the development of molecular theories of complex, multicomponent systems. In the following sections, the most commonly applied dynamical measurements will be described and the theory of PMLRS developed to demonstrate how these moments can be measured experimentally.

The stress tensor

The most commonly measured bulk property associated with the dynamics of polymer liquids is the stress tensor. The polymer contribution to the stress tensor is calculated by considering the stress exerted by polymer segments on planes within the fluid. By properly projecting these forces onto such planes, it can be shown that the stress tensor will be proportional to averages over the probability distribution function in the form of $\sum \langle \boldsymbol{F}_n \boldsymbol{R}_n \rangle$, where $\boldsymbol{F}_n$ is the force exerted by bead n. When Gaussian chain statistics apply, this force is linear in the vector $\boldsymbol{R}_n$ and the stress tensor is:

$$\tau_{ij}^{P} = \frac{3ckT}{b^2} \langle R_i R_j \rangle \tag{1}$$

where c is the number concentration of polymer chains, b is the length of a statistical subunit and the angular brackets represent an average over the probability distribution function. The vector $\boldsymbol{R} = \sum \boldsymbol{R}_n$ shown in *Figure 1* is the end-to-end vector of the chain. The second-order moment, $\langle \boldsymbol{RR} \rangle$, therefore, is an important dynamical quantity in polymer melts.

The refractive index tensor

Another bulk property that is often studied is the refractive index tensor, n_{ij}. This is related to the polarizability tensor, α_{ij}, by the Clausius–Mossotti equation[6]. The polarizability tensor of a polymer liquid will be the sum of the segmental polarizabilities, averaged over the conformational distribution function and can be shown to be:

$$\alpha_{ij} = \bar{\alpha}\delta_{ij} + c\frac{2}{5}\left(\frac{3}{2Nb^2}\right)^2 (\alpha_1 - \alpha_2)\langle R_i R_j \rangle \tag{2}$$

where $(\alpha_1 - \alpha_2)$ is the intrinsic anisotropy in the polarizability of a polymer segment and $\bar{\alpha}$ is the mean polarizability. The fact that both the stress and polarizability tensors are proportional to the second-moment tensor, $\langle \boldsymbol{RR} \rangle$, leads to a linear relationship between the optical and mechanical responses of many polymer liquids, known as the stress-optical rule. This states that the refractive index tensor is simply related to the stress tensor by:

$$n_{ij} = C\tau_{ij} \tag{3}$$

where C is the stress-optical coefficient and is:

$$C = \frac{2\pi}{45kT}\frac{(n^2+2)^2}{n}(\alpha_1 - \alpha_2) \tag{4}$$

Here n is the mean refractive index of the system.

This relationships holds for the *intrinsic* contribution to the refractive index tensor when Gaussian statistics apply. Form effects, due to scattering of light, will not follow this relationship. It is important to note that the stress-optical relationship will apply to both the real and imaginary parts of the refractive index tensor. That is, either birefringence (anisotropy in the real part of the refractive index) or dichroism (anisotropy in the imaginary part) measurements will obey the stress-optical rule.

Raman scattering by polymer liquids

Raman scattering refers to scattered radiation that arises from the interaction between normal vibrational modes of a molecule and radiation-induced oscillating electric dipoles. The electric vector of the scattered light is related to that of the incident light by:

$$E_{iS} = \alpha'_{ij} E_{j0} \tag{5}$$

where E_{j0} is the electric vector of the incident light and α'_{ij} is the Raman tensor of a scattering element; index notation is implied.

If the incident and scattered light have polarizations oriented along the unit vectors l'_i and l'_j, respectively, then the observed intensity of the scattered light is given by:

$$I = I_0 \left\langle \left(\sum_N l'_i l'_j \alpha'_{ij} \right)^2 \right\rangle \tag{6}$$

where I_0 is a constant dependent on the incident light intensity and instrumental factors.

If the frequency of the incident light is removed from an absorption frequency of the sample the classical theory of Raman scattering applies. This theory predicts the following relationship between the Raman tensor and the polarizability tensor[9]:

$$\alpha'_{ij} = \left(\frac{\partial \alpha_{ij}}{\partial Q_k}\right)_0 Q_k \tag{7}$$

where Q_k is a normal mode associated with the kth vibrational mode and the subscript 0 refers to differentials of the polarizability tensor, α_{ij}, about equilibrium configurations. The Raman tensor can therefore be expected to be a function of the end-to-end vector, $\boldsymbol{R}$, of a polymer chain. In general, this tensor will have the

following form for small deformations:

$$\alpha'_{ij} = \eta(\delta_{ij} + \varepsilon R_i R_j) \quad (8)$$

where ε and η are scalar constants. This result can be inserted in equation (6) to obtain a prediction of the Raman scattered light intensity as a function of polymer chain conformation. From equations (6) and (7), it is clear that the Raman experiment will produce measures of the fourth-order moment, $\langle \boldsymbol{RRRR} \rangle$, as well as the second-order moment, $\langle \boldsymbol{RR} \rangle$.

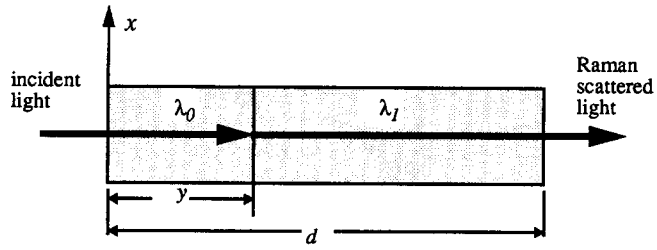

Figure 3 Model of a birefringent sample subject to Raman scattering

POLARIZATION-MODULATED LASER RAMAN SCATTERING: THEORY

Figure 2 is a schematic diagram depicting the geometry of a typical Raman scattering experiment employing polarization modulation. In this case modulation is accomplished by a photo-elastic modulator (PEM) oriented at 45° with respect to the x axis. Preceding that element is a polarizer oriented parallel to the x axis. The PEM induces a sinusoidal retardation of the phase of the transmitted light polarization:

$$\delta'_{\mathrm{PEM}} = A \sin(\omega t) \quad (9)$$

where A is the adjustable peak-to-peak retardance and ω is the fixed frequency of the modulation (typically of the order of 50 kHz).

To calculate the intensity of the Raman scattered light for this or any experimental arrangement, equation (6) can be used. However, it is often more convenient to use Jones or Mueller calculus[10]. With these schemes, the electric vector following a train of optical elements numbered from $m = 1$ to M is:

$$\boldsymbol{E}_M = \boldsymbol{J}_M \boldsymbol{J}_{M-1} \ldots \boldsymbol{J}_1 \boldsymbol{E}_0 \quad (10)$$

or

$$\boldsymbol{S}_M = \boldsymbol{M}_M \boldsymbol{M}_{M-1} \ldots \boldsymbol{M}_1 \boldsymbol{S}_0 \quad (11)$$

where $\boldsymbol{E}_m$and $\boldsymbol{S}_m$ are the electric and Stokes vectors describing the polarization of the light exiting the mth optical component in the train. The incident light polarization is described by $\boldsymbol{E}_0$ and $\boldsymbol{S}_0$. For perfectly polarized light, the Stokes vector is directly related to the Jones vector and has components (for light propagating along the y axis):

$$\boldsymbol{S} = ((|E_x|^2 + |E_z|^2), (|E_x|^2 - |E_z|^2), 2\,\mathrm{Re}(E_x^* E_z), 2\,\mathrm{Im}(E_x^* E_z))^{\mathrm{T}} \quad (12)$$

The matrices $\boldsymbol{J}_m$ and $\boldsymbol{M}_m$ are the Jones and Mueller matrices that describe the linear transformation of the electric vector induced by component m. These two matrices are related in a simple way, although it is generally easier to develop the Jones matrix for a given optical element and then convert it to a Mueller matrix. The Mueller matrix calculation has the advantage of producing observable quantities directly. Since it involves the Stokes vector, it can also describe light that is partially polarized. When the Jones calculus is used, the intensity of light must be determined using $I = |\boldsymbol{E}.\boldsymbol{E}^*|$. Jones and Mueller matrices for polarizers and photo-elastic modulators are found in the Appendix. The appropriate matrices for Raman scattering from oriented samples are developed here for the particular case of zero-angle (or 180°) scattering.

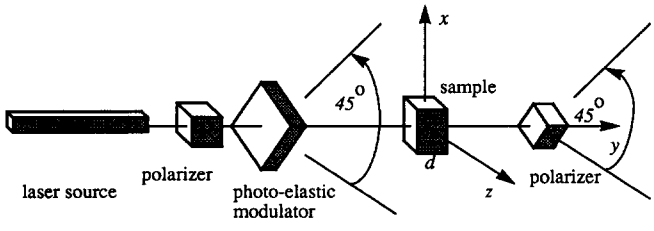

Figure 2 Schematic of the basic polarization-modulated Raman scattering experiment

The calculation of the Jones and Mueller matrices for a Raman scattering element is complicated by the fact that invariably the Raman scattering site is situated within a birefringent material. Since scattering sites will be distributed uniformly throughout the thickness of the specimen, one has to account carefully for the integrated effect of the birefringence.

The model used in this calculation is pictured in *Figure 3*. Here light of wavelength λ_0 is incident on a sample of thickness d. After penetrating the sample a distance y, the light is scattered by a Raman scattering element and exits with wavelength λ_1. Multiple scattering events are neglected and the oriented sample is taken to have a birefringence Δn that is independent of wavelength. Given the relatively small wavelength changes associated with Raman scattering and the weak wavelength dependence of the real part of the refractive index in the visible spectrum, this is a reasonable assumption. The principal axes of the real part of the refractive index tensor in the (x, z) plane are taken to be coincident with the x and z axes, although this restriction can be easily removed.

If light of polarization $\boldsymbol{E}_0$ enters the sample, the electric vector of the Raman scattered light exiting the sample is given by:

$$\boldsymbol{E} \equiv \frac{1}{d}\int_0^d \times \mathrm{d}y \begin{bmatrix} \exp[\mathrm{i}\delta\gamma(d-y)/2d] & 0 \\ 0 & \exp[(-\mathrm{i})\delta\gamma(d-y)/2d] \end{bmatrix} \times \begin{bmatrix} \alpha'_{xx} & \alpha'_{xz} \\ \alpha'_{xz} & \alpha'_{zz} \end{bmatrix} \begin{bmatrix} \exp[\mathrm{i}\delta\gamma/2d] & 0 \\ 0 & \exp[(-\mathrm{i})\delta\gamma/2d] \end{bmatrix} \boldsymbol{E}_0 = \boldsymbol{J}_{\mathrm{Raman}} \boldsymbol{E}_0 \quad (13)$$

where:

$$\delta = 2\pi\,\Delta n d/\lambda_0 \qquad \gamma = \lambda_0/\lambda_1 \quad (14)$$

After carrying out the integrations in equation (13), the elements of the Jones matrix for this particular

scattering geometry are found to be:

$$\begin{aligned} J_{11} &= \alpha'_{xx} \exp\left[i\frac{\delta}{2}\left(1-\frac{\beta}{2}\right)\right] S\left(\frac{\beta\delta}{4}\right) \\ J_{22} &= \alpha'_{22} \exp\left[(-i)\frac{\delta}{2}\left(1-\frac{\beta}{2}\right)\right] S\left(\frac{\beta\delta}{4}\right) \\ J_{12} &= \alpha'_{xz} \exp\left[(-i)\frac{\delta}{4}\beta\right] S\left(\frac{\delta(2-\beta)}{4}\right) \\ J_{21} &= \alpha'_{xz} \exp\left[i\frac{\delta}{4}\beta\right] S\left(\frac{\delta(2-\beta)}{4}\right) \end{aligned} \quad (15)$$

The parameter β is given by:

$$\beta = (\lambda_1 - \lambda_0)/\lambda_1 \quad (16)$$

and is normally a small number. The function $S(\alpha) = (\sin\alpha)/\alpha$. The components of the Mueller matrix for this sample are easily calculated from the Jones matrix components and are tabulated in the Appendix. Once the Jones and Mueller matrices are known, the light intensity for a given experiment can be easily calculated using either equation (10) or (11).

To demonstrate how this is done, let us analyse the PMLRS experiment depicted in *Figure 4*. This experiment has been built in our laboratory and is described in detail in the next section. In this case the intensity measured by the photomultiplier tube (PMT) is determined to be:

$$I/I_0 = R_{dc} + R_{\omega t}\sin[A\sin(\omega t)] + R_{2\omega t}\cos[A\sin(\omega t)] \quad (17)$$

where:

$$R_{dc} = \tfrac{1}{2}(\langle\alpha'^2_{xx}\rangle + \langle\alpha'^2_{zz}\rangle)S^2(\beta\delta/4) + \langle\alpha'^2_{xz}\rangle S^2(\delta(2-\beta)/4) \quad (18)$$

$$R_{\omega t} = \langle\alpha'_{xx}\alpha'_{zz}\rangle\{S^2(\beta\delta/4)\sin[\delta(1-\beta/2)]\} + \langle\alpha'^2_{xz}\rangle[S^2(\delta(2-\beta)/4)\sin(\beta\delta/2)] \quad (19)$$

$$R_{2\omega t} = \tfrac{1}{2}(\langle\alpha'^2_{xx}\rangle - \langle\alpha'^2_{zz}\rangle)S^2(\beta\delta/4) \quad (20)$$

The time-dependent terms arising from the photoelastic modulation can be expanded in the following Fourier series:

$$\cos[A\sin(\omega t)] = J_0(A) + 2\sum_{n=1}^{\infty} J_{2n}(A)\cos(2n\omega t) \quad (21)$$

$$\sin[A\sin(\omega t)] = 2\sum_{n=0}^{\infty} J_{2n+1}(A)\sin[(2n+1)\omega t] \quad (22)$$

The modulator can be adjusted so that its amplitude leads to the condition $J_0(A) = 0$. Rewriting equation (17) so that only the leading-order terms in the Fourier expansion are retained leads to:

$$\frac{I}{\eta^2 I_0} = \tfrac{1}{4}[R_{dc} + 2J_1(A)R_{\omega t}\sin(\omega t) + 2J_2(A)R_{2\omega t}\cos(2\omega t)] \quad (23)$$

The averages of the squares of the components of the Raman scattering tensor listed in equations (18) to (20) can be related to moments of the orientation distribution function using equation (8). Making this substitution and retaining terms up to $O(\beta)$ leads to the following expressions:

$$R_{dc} = 1 + \varepsilon(\langle x^2\rangle + \langle z^2\rangle) + \tfrac{1}{2}\varepsilon^2(\langle x^4\rangle + \langle z^4\rangle) + \varepsilon^2 S^2(\delta/2)\{1 + \beta[1 - \tfrac{1}{2}\delta\cot(\delta/2)]\}\langle x^2z^2\rangle \quad (24)$$

$$R_{\omega t} = (\sin\delta - \tfrac{1}{2}\beta\delta\cos\delta) \times [1 + \varepsilon(\langle x^2\rangle + \langle z^2\rangle) + \varepsilon^2\langle x^2z^2\rangle] + \tfrac{1}{2}\delta S^2\beta(\delta/2)(\varepsilon^2\langle x^2z^2\rangle) \quad (25)$$

$$R_{2\omega t} = \varepsilon(\langle x^2\rangle - \langle z^2\rangle) + \tfrac{1}{2}\varepsilon^2(\langle x^4\rangle - \langle z^4\rangle) \quad (26)$$

Similarly the intensity measured by the birefringence detector can be shown to be:

$$I/I_0 = R_{dc,b} + 2J_1(A)R_{\omega t,b}\sin(\omega t) \quad (27)$$

where:

$$R_{dc,b} = \tfrac{1}{4} \quad (28)$$

$$R_{\omega t,b} = \tfrac{1}{4}\sin\delta \quad (29)$$

The ratios R_{dc}, $R_{\omega t}$, $R_{2\omega t}$, $R_{dc,b}$ and $R_{\omega t,b}$ can be determined with the use of low-pass filters and phase-sensitive detectors interfaced with lock-in amplifiers, locked to $\sin(\omega t)$ and $\cos(2\omega t)$. It is apparent that the birefringence of the sample must be simultaneously measured in order to analyse the results properly.

The experiment described above is only one example of a configuration that can be analysed in this way. Similar expressions can be derived for the case where the scattered light is measured along the z axis, for example. Various orientations of the analysing polarizer can also be considered. For example, let us consider an experiment where no modulation is applied and the backscattered Raman light is observed through a polarizer oriented at an angle of 90° relative to the polarization direction of the incident light. It is straightforward to show that in this case the intensity is:

$$\frac{I}{\eta^2 I_0} = \frac{\varepsilon^2}{4}\left\{\langle x^2z^2\rangle\left[\left(\frac{1-\cos\delta}{(\delta/2)^2}\right) \times \{1 + \beta[1 - \tfrac{1}{2}\delta\cot(\delta/2)]\}\right]\right\} \quad (30)$$

which again indicates that it is necessary to take into account the integrated effect of the sample's birefringence in analysing even this relatively simple experiment. It is clear, however, that for very small values of the retardation the predicted intensity becomes identical to the intensity that would be calculated if the birefringence of the sample is neglected. On the other hand, if the analyser orientation is 0° relative to the polarization direction of the incident light, the intensity is determined to be:

$$I/\eta^2 I_0 = \tfrac{1}{2}(1 + 2\varepsilon\langle x^2\rangle + \varepsilon^2\langle x^4\rangle) \quad (31)$$

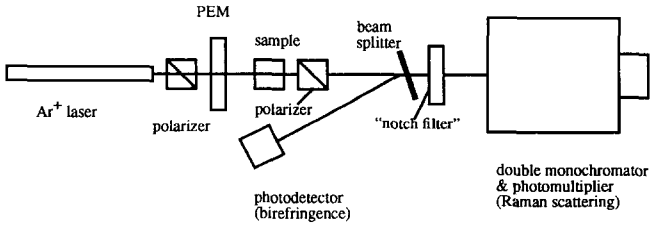

Figure 4 Experimental arrangement for simultaneous measurement of birefringence and PMLRS

In this case it is evident that the birefringence of the specimen has no observable effect on the Raman scattered light.

EXPERIMENTAL

Apparatus

To test the feasibility of PMLRS, the experiment shown in *Figure 4* has been built. It consists of an argon ion laser (Lexel) operating at approximately 120 mW of power at 514 nm. Polarization modulation is accomplished using a polarizer and photo-elastic modulator (Hinds International) at a relative orientation of 45°. Flow is generated either by stretching the sample between the jaws of a simple stretching cell, or by shearing it between glass plates in a parallel-plate flow cell. Following the sample, the light is passed through an analysing polarizer oriented at 45° and then split using a glass window held at a small angle of incidence. The transmitted light is sent through a narrow-band 'notch' filter (Omega Optical) that removes the laser line, and then through a Spex 1680-SS double monochromator. The intensity is then measured using a R928 photo-multiplier tube in a cooled housing (Thorn EMI).

The light reflected by the beam splitter is used to measure the birefringence of the sample, which, as demonstrated previously, is required for the analysis of the Raman scattering signals. The signals from both detectors are sent simultaneously to low-pass filters and lock-in amplifiers. The former permits the d.c. signals to be measured, while the latter determines the relevant Fourier components of each intensity signal.

Materials and experimental protocol

Using the experimental system described in the previous section, a number of flow experiments were conducted. The polymer sample used was a polyisobutylene melt with an average molecular weight of 380000. This polymer is transparent and is a room-temperature melt, although the molecular weight is sufficiently large so that it could be handled much like an elastomer. Two types of experiments were performed, both using the Raman scattered light associated with the symmetric stretching vibration of the C–H groups present in the sample ($\sim$2960 cm^{-1} or $\sim$604 nm). The Raman spectrum for this material is shown in *Figure 5*.

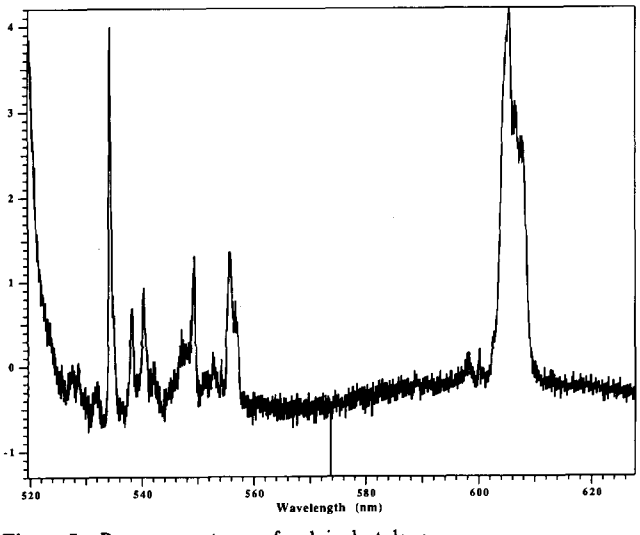

Figure 5 Raman spectrum of polyisobutylene

In the first case, uniaxial step strain deformations of samples in the form of sheets, 4.0 mm thick, were applied (at room temperature) by simply fastening the specimen between one stationary and one movable clamp of a simple stretching cell. The drive used consisted of a stepper motor that could be precisely controlled to subject the sample to a specified strain. The stretching protocol consisted of two successive step strains, the second being in the opposite direction to the first, with a delay time of 12 s between the two displacements. Five signals were recorded simultaneously as a function of time: R_{dc}, $R_{\omega t}$, $R_{2\omega t}$, for the Raman scattering measurement, and two similar signals for the birefringence measurement. The second type of experiment consisted of a step strain deformation where the sample was sandwiched between parallel glass plates, one fixed and one movable, in a shear flow cell. The sandwiched sample was approximately 0.75 mm thick. Step strain deformations were accomplished by moving one of the plates relative to the other. The drive consisted of a stepper motor. In this case the sample was heated to 80°C and subjected to a single step strain of 100%.

Results and discussion

Figures 6a through *6d* summarize the results obtained for the stretching experiments. Here the signal ratios following step reversal extensions for a number of stretch ratios (ε) are plotted as a function of time. From *Figure 6a* it is evident that the response of R_{dc} is flat and independent of the stretch ratio. This is expected since, for the stretch ratios employed, the orientation-independent part of the Raman tensor is much larger than the orientation-dependent part. This is confirmed by the fact that the response of $R_{\omega t}$ is very similar in form to the birefringence response (R_{biff}), which, from equation (25), is only expected if the above is true, given that β is a small number ($\beta = 0.15$ in this case). This similarity is particularly evident in the oscillations in both of these signal ratios at 24% strain. These are a manifestation of the fact that the retardation due to birefringence in the sample (δ defined in equation (14)) becomes greater than $\pi/2$. On the other hand, the response of $R_{2\omega t}$ is independent of the sample's birefringence, which is expected from equation (26). Moreover, since this signal depends, to leading order, on the anisotropy of both the second-order and fourth-order moments of the orientation distribution function, it is a direct measure of the time dependence of these moments. However, even though it is in principle possible to solve equations (24) through (26) simultaneously, to obtain signal ratios that reflect the independent time dependence of each of these moments, this is not possible in this case. The reason for this is that both the measured R_{dc} and $R_{\omega t}$ signals are independent of the moments. In its present form, the experiment can only provide the fourth-order moments if the $O(\varepsilon)$ and $O(\varepsilon^2)$ terms in R_{dc} and $R_{\omega t}$ are measurable. At the strains imposed in these experiments, these terms are too small to be determined. A possible solution to this problem, which we are currently pursuing, is the development of modulation schemes that would eliminate the dependence of $R_{\omega t}$ on the orientation-independent part of the Raman tensor.

It is also noteworthy that $R_{2\omega t}$ does not oscillate at 24% strain. This is expected since it does not involve a trigonometric dependence on the anisotropy as in the case of the birefringence measurement. This represents

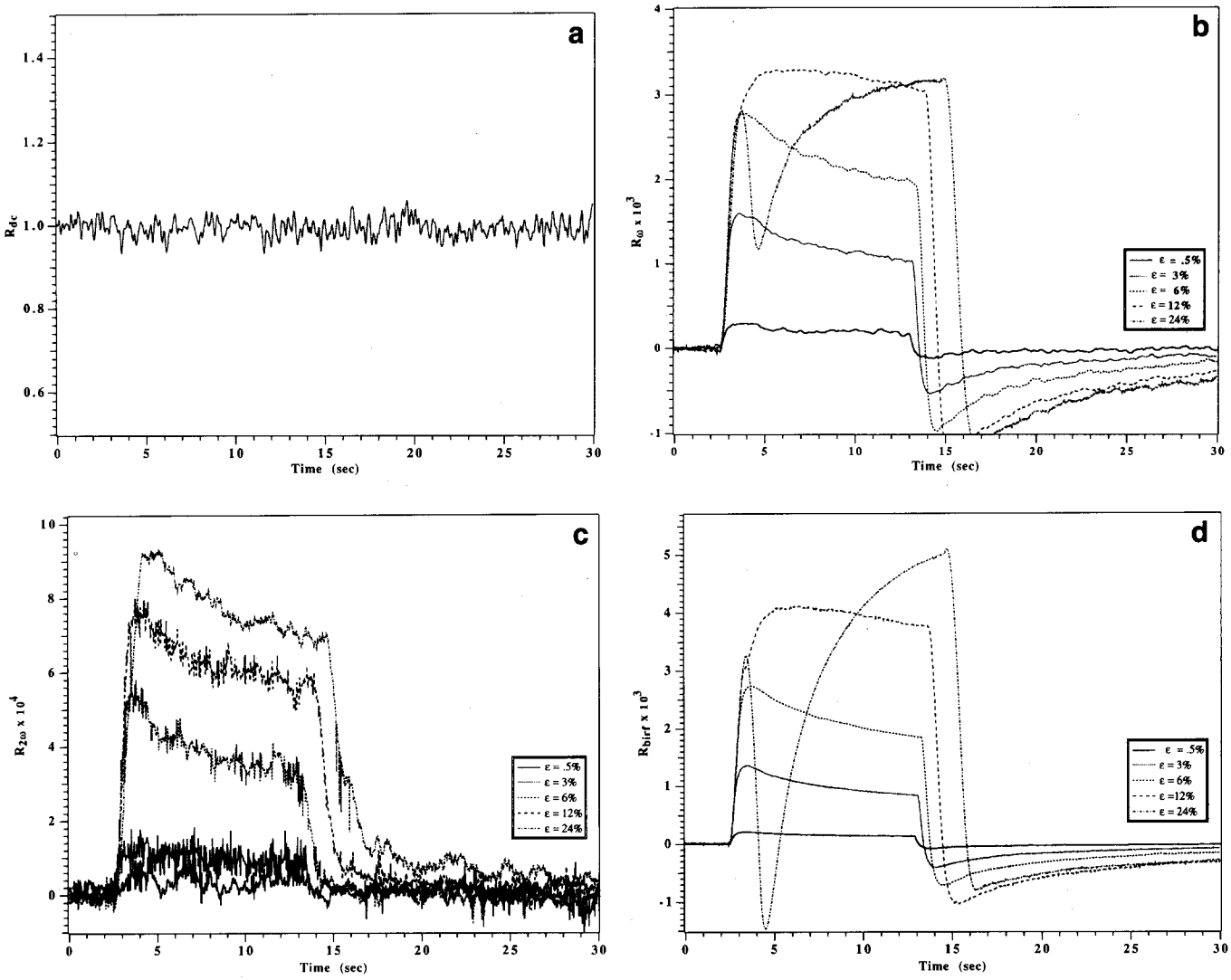

Figure 6 Plots of signal ratios following single step reversal ranging from 0.5% to 24%: (a) R_{dc}, (b) $R_{\omega t}$, (c) $R_{2\omega t}$ and (d) R_{birf}

an important advantage of PMLRS over birefringence and dichroism measurements for polymer melts where large retardations and extinctions frequently occur. Multiple orders in retardation can make the unambiguous determination of birefringence very difficult and time-consuming.

The results obtained for the step strain experiments are summarized in *Figures 7a* through *7e*. Here the signal ratios following a single step strain deformation of 100% are plotted as a function of time. From *Figure 7a* it is evident that the response of R_{dc} is again flat, suggesting that even at this relatively high strain the moments are still much smaller than the orientation-independent term (equation (24)). Comparing the strain used in this experiment with the strain at which the birefringence goes through orders, in the extension experiments, one is inclined to expect R_{birf} and $R_{\omega t}$ also to go through orders. However, *Figures 7b* and *7d* indicate no such behaviour. The reason for this is that the thickness of the sample used in this experiment is much smaller than that used in the extension experiments; the retardation will be correspondingly smaller. Single-exponential fits to $R_{\omega t}$ and R_{birf} yield long-time characteristic relaxation times of 25.3 s and 25.7 s respectively. The agreement between these values is quite good, which is not surprising because from equation (25) and *Figure 7a* we expect the $R_{\omega t}$ signal to be dominated by the response of the sample birefringence to the step strain deformation. *Figure 7e* is a plot of the retardation δ (recovered from R_{birf}) as a function of time. The retardation is proportional to the anisotropy in the second-order moments and is therefore expected to yield similar information to $R_{2\omega t}$ about the relaxation dynamics. Single-exponential fits to $R_{2\omega t}$ and the retardation yield characteristic relaxation times of 21.6 s and 24.8 s respectively. Given the relatively poor signal-to-noise ratio of the $R_{2\omega t}$ signal, the agreement between these two relaxation times is quite reasonable.

CONCLUSIONS

These results demonstrate that PMLRS can successfully produce measures of the time-dependent orientation of molecular segments in polymer liquids. In addition, because it is a spectroscopic technique, it can also provide information about the orientation dynamics of specific segments on a polymer chain, or specific components in a blend of dissimilar polymers. The theoretical approach developed accurately describes what is observed experimentally. However, at this point it is not clear whether it will be possible to determine the relaxation of the

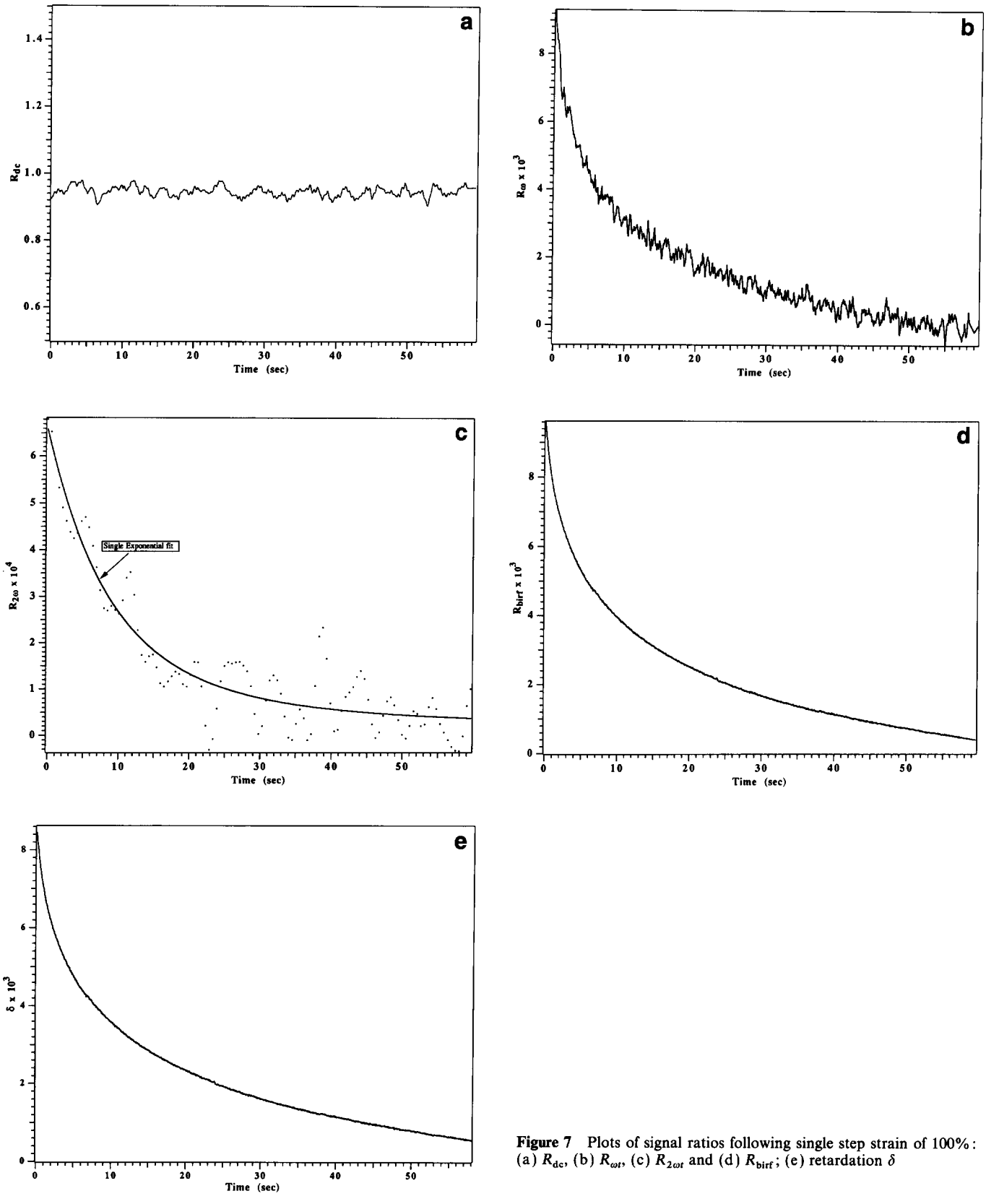

Figure 7 Plots of signal ratios following single step strain of 100%: (a) R_{dc}, (b) $R_{\omega t}$, (c) $R_{2\omega t}$ and (d) R_{birf}; (e) retardation δ

second-order and fourth-order moments of the orientation distribution function independently of each other, without deforming the sample beyond the limits capable of being described by current viscoelasticity theories. Here, it is instructive to point out that previous studies that have been successful in determining both second- and fourth-order moments have employed stretch ratios ranging from 100% to 500%[2,3].

It is also possible that other optical arrangements (such as 90° scattering) might be advantageous. Certainly scattering geometries other than the forward scattering example presented here need to be considered when deformations other than simple uniaxial extension are applied. If simple shearing deformations are used, for example, it will be necessary to consider both forward and 90° scattering with the incident light propagating

either along the gradient axis (the y axis) or along the vorticity axis (the z axis) since each case will provide different combinations of second- and fourth-order moments. If the shear flow is defined by the velocity field $\boldsymbol{u} = (\dot{\gamma}y, 0, 0)$, forward scattering with the incident light sent parallel to the y axis will provide moments that are combinations of $\langle x^2 \rangle$, $\langle z^2 \rangle$, $\langle x^4 \rangle$ and $\langle z^4 \rangle$. If the scattered light is measured along the z axis, on the other hand, moments of the form of $\langle xy \rangle$ and $\langle x^2 y^2 \rangle$ will be measured along with moments that are combinations of $\langle x^2 \rangle$, $\langle y^2 \rangle$, $\langle x^4 \rangle$ and $\langle y^4 \rangle$. As indicated previously, various modulation schemes will also be investigated as well as different designs for the analysing optics.

ACKNOWLEDGEMENTS

This project is supported by research grants from IBM and the NSF–MRL Center for Materials Research at Stanford. We would also like to thank Mr Volker Abetz and Mr Douglas Werner for insightful discussions during the course of this work.

REFERENCES

1 Bower, D. I. *J. Polym. Sci., Polym. Phys. Edn.* 1972, **10**, 2135
2 Purvis, J. and Bower, D. I. *J. Polym. Sci., Polym. Phys. Edn.* 1976, **14**, 1461
3 Maxfield, J., Stein, R. S. and Chen, M. C. *J. Polym. Sci., Polym. Phys. Edn.* 1978, **16**, 38
4 Purvis, J. and Bower, D. I. *Polymer* 1974, **15**, 645
5 Satija, S. and Wang, C. H. *J. Chem. Phys.* 1978, **69**, 2739
6 Doi, M. and Edwards, S. F. 'The Theory of Polymer Dynamics', Oxford University Press, New York, 1986
7 Larson, R. G. 'Constitutive Equations for Polymer Melts and Solutions', Butterworths, Boston, 1988
8 Bird, R. B., Hassager, O., Armstrong, R. C. and Curtiss, C. F. 'Dynamics of Polymeric Liquids', Wiley, New York, 1977, Vol. 2
9 Long, D. A. 'Raman Spectroscopy', McGraw-Hill, London, 1977
10 Azzam, R. M. A. and Bashara, N. M. 'Ellipsometry and Polarized Light', North-Holland, New York, 1977

APPENDIX

Jones matrices

Ideal polarizer oriented at α*:*

$$\begin{pmatrix} c_\alpha^2 & c_\alpha s_\alpha \\ c_\alpha s_\alpha & s_\alpha^2 \end{pmatrix}$$

where $c_\alpha = \cos(\alpha)$ and $s_\alpha = \sin(\alpha)$ etc.

Birefringent element with retardation δ *oriented at* α*:*

$$\begin{pmatrix} c_{\delta/2} - \mathrm{i}c_{2\alpha}s_{\delta/2} & -\mathrm{i}s_{2\alpha}s_{\delta/2} \\ -\mathrm{i}s_{2\alpha}s_{\delta/2} & c_{\delta/2} + \mathrm{i}c_{2\alpha}s_{\delta/2} \end{pmatrix}$$

where for a PEM, $\delta = A\sin(\omega t)$, ω being the modulation frequency.

Mueller matrices

Ideal polarizer oriented at α*:*

$$\frac{1}{2}\begin{pmatrix} 1 & c_{2\alpha} & s_{2\alpha} & 0 \\ c_{2\alpha} & c_{2\alpha}^2 & c_{2\alpha}s_{2\alpha} & 0 \\ s_{2\alpha} & c_{2\alpha}s_{2\alpha} & s_{2\alpha}^2 & 0 \\ 0 & 0 & 0 & 0 \end{pmatrix}$$

Birefringent element with retardation δ *oriented at* α*:*

$$\begin{pmatrix} 1 & 0 & 0 & 0 \\ 0 & c_{2\alpha}^2 + s_{2\alpha}^2 c_\delta & c_{2\alpha}s_{2\alpha}(1 - c_\delta) & s_{2\alpha}s_\delta \\ 0 & c_{2\alpha}s_{2\alpha}(1 - c_\delta) & s_{2\alpha}^2 + c_{2\alpha}^2 c_\delta & -c_{2\alpha}s_\delta \\ 0 & -s_{2\alpha}s_\delta & c_{2\alpha}s_\delta & c_\delta \end{pmatrix}$$

Mueller matrix components for Raman scattering element in birefringent medium (0° scattering; direction of propagation y*):*

$$M_{11} = \eta^2\{S^2(\beta\delta/4)[1 + \varepsilon(\langle x^2 \rangle + \langle z^2 \rangle) + \tfrac{1}{2}\varepsilon^2(\langle x^4 \rangle + \langle z^4 \rangle)] + S^2(\delta(2 - \beta)/4)\varepsilon^2\langle x^2 z^2 \rangle\}$$

$$M_{12} = \eta^2\{S^2(\beta\delta/4)[\varepsilon(\langle x^2 \rangle - \langle z^2 \rangle) + \tfrac{1}{2}\varepsilon^2(\langle x^4 \rangle - \langle z^4 \rangle)]\} = M_{21}$$

$$M_{13} = M_{31} = M_{14} = M_{41} = 0$$

$$M_{22} = \eta^2\{S^2(\beta\delta/4)[1 + \varepsilon(\langle x^2 \rangle + \langle z^2 \rangle) + \tfrac{1}{2}\varepsilon^2(\langle x^4 \rangle + \langle z^4 \rangle)] - S^2(\delta(2 - \beta)/4)\varepsilon^2\langle x^2 z^2 \rangle\}$$

$$M_{23} = M_{32} = M_{24} = M_{42} = 0$$

$$M_{33} = \eta^2\{S^2(\beta\delta/4)\cos(\delta - \beta\delta/2) \times [1 + \varepsilon(\langle x^2 \rangle + \langle z^2 \rangle) + \varepsilon^2\langle x^2 z^2 \rangle] + S^2(\delta(2 - \beta)/4)\cos(\beta\delta/2)\varepsilon^2\langle x^2 z^2 \rangle\}$$

$$M_{43} = -M_{34} = \eta^2\{S^2(\beta\delta/4)\sin(\delta - \beta\delta/2) \times [1 + \varepsilon(\langle x^2 \rangle + \langle z^2 \rangle) + \varepsilon^2\langle x^2 z^2 \rangle] + S^2(\delta(2 - \beta)/4)\sin(\beta\delta/2)\varepsilon^2\langle x^2 z^2 \rangle\}$$

$$M_{44} = \eta^2\{S^2(\beta\delta/4)\cos(\delta - \beta\delta/2) \times [1 + \varepsilon(\langle x^2 \rangle + \langle z^2 \rangle) + \varepsilon^2\langle x^2 z^2 \rangle] - S^2(\delta(2 - \beta)/4)\cos(\beta\delta/2)\varepsilon^2\langle x^2 z^2 \rangle\}$$

where $S(x) = (\sin x)/x$ and $\beta = (\lambda_1 - \lambda_0)/\lambda_1$; λ_0 being the wavelength of the incident light and λ_1 the wavelength of the Raman scattered light.